JOURNAL OF MATERIALS SCIENCE **39** (2004) 5023–5029

# Phase transformations in nanocrystalline alloys synthesized by mechanical alloying

C. BANSAL*, S. SARKAR
*School of Physics, University of Hyderabad, Hyderabad 500 046, India*
*E-mail: cbsp@uohyd.ernet.in*

The effect of nanometer grain size and extensive grain boundary regions in nanocrystalline alloy systems was investigated for the chemical order-disorder, structural, precipitation, and spinodal phase transformations.

The kinetic paths for approach to the chemically ordered phase from the disordered phase in FeCo-Mo alloys were observed to be the same at different temperatures due to grain boundaries acting as short-circuited diffusion paths for atom movements. The structure of $Fe_3Ge$ was bcc for small crystallite size and the equilibrium fcc phase developed only after a critical grain size was attained. This was understood as a manifestation of the Gibbs Thomson effect.

The precipitation phase transformation in Fe-Mo alloys proceeded by a rapid movement and clustering of the Mo atoms to the grain boundaries that was correlated to the size of the nano grains, and subsequent formation of the Mo rich lambda phase directly in the grain boundary regions.

The composition fluctuation domains for spinodal decomposition in nanophase Fe-Cr alloys were observed to be linearly correlated to the growth of grains.


## 1. Introduction

It is of interest to study and understand how the small size of the grains as well as the presence of extensive grain boundary regions in nanocrystalline alloys influence their phase transformation behavior as compared to the conventional coarse grained polycrystalline alloys. This is important not only from the viewpoint of a basic understanding of nanophase systems but also for applications to process the materials for desired phases, microstructure, and properties. It is anticipated that in a nanophase alloy there would be enhanced atomic diffusivity through grain boundary regions and the free energy of the system would also be altered due to surface energy contributions [1] and these effects should influence all the metallurgical phase transformations. In this work we present experimental studies on alloy systems that undergo different phase transformations such as chemical order-disorder (FeCo-X, X = Mo, Ge), precipitation (Fe-Mo), structural (Fe-Ge), and spinodal (Fe-Cr), to understand their behavior in the nanocrystalline phase.

## 2. Experimental

The alloys were prepared by mechanical alloying of constituent elemental metal and nonmetal powders (99.99% + purity) in a SPEX 8000 Mixer Mill. The milling was carried out for 24 h (except in the case of FeCo-Mo alloy where a milling time of up to 50 h was required for fully disordered alloy to form) in hardened steel vials using a set of six steel balls, two of diameter $1/2''$ and four of diameter $1/4''$. The vial with the powders and steel balls was sealed under Argon atmosphere in a glove bag and put for milling. The ball to powder weight ratio was 5:1. The Fe contamination due to ball milling was typically about 1 to 2 atomic percent as determined by EDAX and chemical composition analysis. The as-milled alloys were subjected to heat treatments at various temperatures for periods of time ranging from few minutes to few hundreds of hours to see the formation of the equilibrium phases as expected from the phase diagram. The heat treatments were carried out after sealing the samples in borosilicate glass ampoules under argon atmosphere at a pressure of 0.005 Torr. Powder X-ray diffraction studies were carried out to determine the phases and average grain sizes using Scherrer formula. Mössbauer spectroscopy was used to study in detail the disorder-order, precipitation, structural, and spinodal phase transformation behavior of the alloys, all of which were Fe based.

## 3. Results

### 3.1. Disorder-order phase transformations in FeCo-X (X = Mo, Ge)

In a ternary alloy, where the state of order is characterized by two order parameters, the alloy may develop

*Author to whom all correspondence should be addressed.

various combinations of the order parameters in the approach to the final equilibrium state [2]. The initial and final states may be connected by different chains of intermediate states i.e. for a given value of one order parameter, the other order parameter need not have a unique value. It was shown using Master Equation formulation that these chains of kinetic evolution towards the final equilibrium order or '*kinetic paths*' were temperature dependent when the atomic species of the alloy had different activation energy barrier heights for diffusive jumps or different inter atomic interactions.

A Mössbauer spectroscopic study on the kinetics of chemical ordering in several piston-anvil quenched FeCo-X alloys (X = W, Nb, Mo, Cr, Ti, V, and Al) showed that the kinetics of B2 ordering was slowed down for the 4d and 5d solutes but the 3p and 3d series elements did not affect the ordering kinetics [3]. This was understood to arise due to the lesser mobility of the W, Nb and Mo solutes. A more detailed investigation of the FeCo-Mo system was subsequently carried out to observe differences in *kinetic paths* of the Warren-Cowley short-range order parameters $\alpha_{\mathrm{Mo/Fe}}$ and $\alpha_{\mathrm{Co/Fe}}$ at different temperatures [4]. The kinetic paths at 350 and 400°C were indeed observed to be different albeit not as much as predicted from model calculations. The temperature dependence of *kinetic paths* was attributed to the high activation energy barrier for diffusive jumps of Mo atoms.

We studied the kinetics of the evolution of B2 order in ternary FeCo-Mo and FeCo-Ge nanophase alloys to see the new effects related to the grain size and grain boundaries [5, 6]. We observed the presence of satellite lines in FeCo-Mo at lower field values similar to that observed by adding a few atomic percent solutes to pure iron in several Fe-X (where X = few atomic percent Si, Al, Mn, Cr, Mo etc.) alloys [7]. The observed field shift of 54 kOe for the satellite line is in good agreement with earlier work [3]. For the Fe-48 at.% Co-4 at.% Ge as milled sample also we observed a satellite peak, which was attributed to the presence of Ge in the first nn shell of Fe. The shift between the main peak and the 1 Ge nn peak is 24.9 kOe, in good agreement with the field shift of 24 kOe observed in Fe-6 at.% Ge alloy [8].

After ordering heat treatments the width of the main peaks as well as the intensity of the satellite peak decreases. The area of the main peak on the other hand increases. From these observations and also from earlier studies of disorder → B2 order transformation in pure FeCo [9] it is known that the width of the hyperfine distribution decreases with increase in chemical order due to a change in 1nn environment from a random distribution to that of an ordered arrangement of all Co neighbours. The width of the main peak is therefore an appropriate measure of the ⟨Co/Fe⟩ correlation. Similarly as the order develops more and more configurations correspond to Fe atom with Co neighbours and the area of the main peak increases; therefore this area can also be considered as a measure of the ⟨Co/Fe⟩ correlation.

The area of the satellite peak corresponds to the ⟨Mo/Fe⟩ correlation. A decrease in Mo satellite area as ordering takes place shows that Mo atoms move away

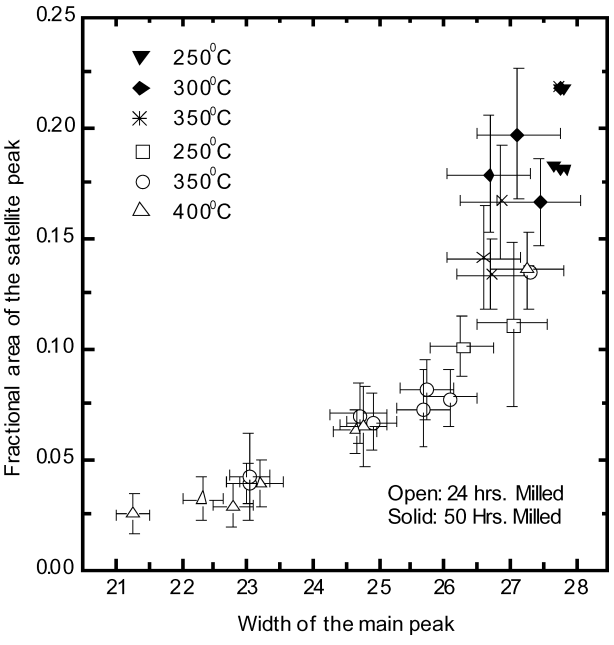


*Figure 1* Kinetic paths for B2 ordering in nanocrystalline FeCo-Mo at different temperatures. The ⟨Co/Fe⟩ and ⟨Mo/Fe⟩ correlations are represented by the width of the main peak and the intensities of the satellite peaks respectively.

from 1nn shell of Fe to a Co near neighbor environment. This is in agreement with the metallic bonding theory of Miedema [10] according to which Co-Mo bonding is preferred to Fe-Mo bonding.

The *kinetic paths* as shown in Fig. 1 for the nanocrystalline FeCo-4 at.% Mo alloy at different temperatures in the space spanned by the order parameters ⟨Mo/Fe⟩ and ⟨Co/Fe⟩ are essentially the same within experimental errors at all the temperatures [5]. Exactly similar results were obtained for the FeCo-Ge nanocrystalline alloy system heat treated at 300, 350 and 400°C [6]. This observation should be compared to the behavior of piston-anvil quenched polycrystalline FeCo-Mo alloys [4] where these *kinetic paths* were seen to be distinctly different at 350 and 400°C. The absolute rate of change of these correlations at these temperatures in nanocrystalline alloys were also seen to be substantially faster as compared to those observed in the previous study [4]. This observation prompted us to study the evolution of order at a lower temperature of 250°C to see whether higher activation barrier for Mo diffusion would give rise to difference in kinetic path at a lower temperature. The rate of change of correlations was observed to be slower, as expected at lower temperature but the kinetic path followed was the same as that at 350 and 400°C. We therefore infer that the kinetic path behavior of the nanocrystalline system is intrinsically related to the nanocrystalline nature of the ball-milled alloys. The main difference between the microcrystalline and nanocrystalline systems is the presence of large volume fraction of grain boundary regions. These boundary regions provide *short-circuited paths* for diffusion of atoms [1, 11]. The activation energy of diffusion for the different atoms along these *short-circuited paths* may not be substantially different and thus give rise to identical *kinetic paths* for ordering.

### 3.2. Precipitation phase transformation in Fe-Mo

The Mössbauer spectra and the corresponding HMF distribution of the as-milled Fe-Mo alloys show the formation of homogenous Fe-Mo solid solutions and there was no evidence for a paramagnetic doublet from the λ phase ($Fe_2Mo$ stoichiometry) that is expected from the phase diagram. The as-milled nanocrystalline alloys were heat treated at 400 and 520°C to see the nano structure evolution and equilibrium phase decomposition behaviour. The depletion of Mo atoms from the near neighbor environment of Fe was observed by measuring the intensities of the satellite lines, which were found to diminish whereas the intensity of the zero Mo peak was found to increase. Correspondingly there was no evidence for growth of Mo rich λ phase in the spectrum. From the phase diagram it was expected that the λ phase should have developed giving rise to a quadrupole split spectrum [12] with no HMF. The absence of the λ phase but the depletion of Mo from the Fe environment shows that Mo clustering is taking place from the $\alpha$ phase. This is in qualitative agreement with the observations of Marcus *et al.* [12, 13] for microcrystalline alloys. However a comparison of the time dependence of the satellite peak intensities for the microcrystalline [12] and nanocrystalline alloys shows them to be different. For the microcrystalline alloys there is no significant decrease in the satellite peak areas up to 2 h of heat treatment after which it starts showing a decrease between 2 and 5 h. For the nanocrystalline system the decrease in satellite peak area is observed to be faster and a significant decrease in intensity takes place even for half an hour of heat treatment. The probable reason for this accelerated clustering of Mo atoms lies in the larger volume fraction of the grain boundary regions in the nanocrystalline systems, which provide faster diffusion paths [5].

We observed an interesting correlation between the grain size and the depletion of Mo atoms from the near neighbor environment of Fe as shown in the parametric plots of Fig. 2. There appears to be a critical size below which the Mo solute atoms remain dissolved in the $\alpha$ phase. This can be attributed to the additional contribution to the Gibbs free energy from the surface energy ($\gamma$) of the nano size grains of radius $R$ in the nanocrystalline phase. This is referred to as a capillary effect or Gibbs Thomson effect [1] and is given by:

$$\Delta G(R) = 2\gamma \mathrm{V_m}/R \qquad (1)$$

where $\mathrm{V_m}$ is the molar volume. The Gibbs free energy of mixing for an alloy system comprising of crystallites of finite size $R$ will contain an additional term $\Delta G(R)$ from the surface energy contribution (Equation 1)

$$\Delta G_{\mathrm{mix}} = \Delta U_{\mathrm{mix}} - T\Delta S_{\mathrm{mix}} + \Delta G(R) \qquad (2)$$

where $\Delta U_{\mathrm{mix}}$ and $\Delta S_{\mathrm{mix}}$ are internal energy and entropy of mixing and $T$ is the temperature. In a system such as Fe-Mo with positive internal energy of mixing ($\Delta U_{\mathrm{mix}}$) the bond energies satisfy $E_{\mathrm{AA}} + E_{\mathrm{BB}} < 2E_{\mathrm{AB}}$. A solid solution of Fe and Mo at a temperature

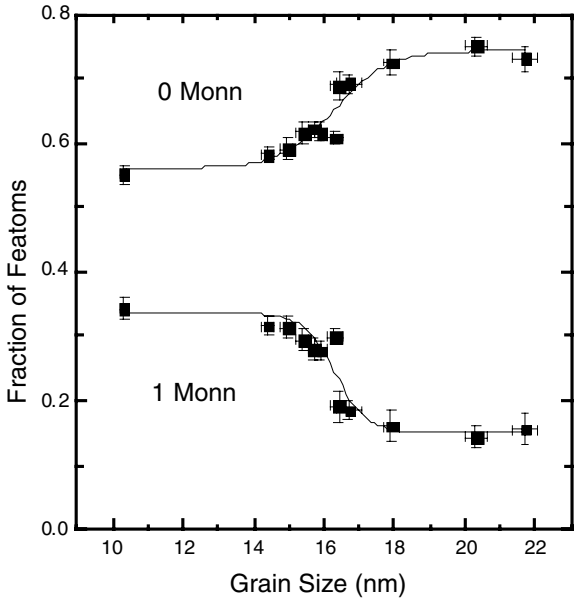


*Figure 2* Change in the near neighbor environment of Fe due to Mo precipitation plotted as a function of grain size.

below the solvus temperature would therefore be possible for nanosize grains if the surface energy term is negative (implying negative $\gamma$) and compensates the positive internal energy of mixing to give $\Delta G_{\mathrm{mix}} \leq 0$. In nanocrystalline alloys prepared by mechanical alloying the grain boundaries are predominantly high angle grain boundaries, which have a relatively open structure and large free volume. The bonds between the atoms in these high angle grain boundaries are broken [1]. Mo or Fe atoms residing in the grain boundary regions will therefore have lower energy as compared to that of Mo or Fe atoms within the grain because of less number of repulsive Fe-Mo bonds. The surface energy ($\gamma$) can therefore be negative. This situation is in contrast to systems with a negative internal energy of mixing where the broken bonds in high angle grain boundary regions have a positive surface energy because of a decrease in the number of attractive AB bonds. Because of the inverse $R$ dependence of $\Delta G(R)$ there exists a radius $R_{\mathrm{o}}$ up to which $\Delta G_{\mathrm{mix}}$ remains negative and beyond which the free energy of mixing $\Delta G_{\mathrm{mix}}$ becomes positive and the solute starts to separate from the solid solution. $R_{\mathrm{o}}$ is obtained by equating $\Delta G_{\mathrm{mix}}$ in Equation 3 to zero. This gives

$$R_{\mathrm{o}} = 2\gamma V_{\mathrm{m}}/\Delta S_{\mathrm{mix}}(T - T_{\mathrm{o}}) \qquad (3)$$

where $T_{\mathrm{o}}$ is the solvus temperature, $T$ is the temperature at which the precipitation transformation is experimentally observed, and we have taken $\Delta U_{\mathrm{mix}} \cong \Delta H_{\mathrm{mix}} = T_{\mathrm{o}}\,\Delta S_{\mathrm{mix}}$. An estimate of the grain size at which the solute atoms start separating from the solution is possible if the value of $\gamma$ is known. However if we assume a typical value for $|\gamma|$ of about 200 mJ/m$^2$ [Ref. [1], p. 155], this grain size comes out to be about 16 nm at 520°C for Fe-5 at.% Mo alloy. This estimate appears to be in agreement with our experimental observations (Fig. 2). Similar behavior of Mn segregation to grain boundaries has also been observed in our measurements on Mn substituted Fe-Si nanocrystalline alloys [14].

However the location of the Mo clusters seemed to be different in the nano system as compared to the microcrystalline system. In the microcrystalline system there was once again an increase in the satellite peak area between 20 and 250 h, after which the Mo rich $\lambda$ phase started forming. The initial decrease followed by an increase in satellite peak intensity after 20 h of heat treatment implies that Mo clusters, which may have been precipitated within the grains, are once again dissolved in the Fe matrix before the $Fe_2Mo$ phase is formed. In contrast our nanocrystalline alloys show no reentrant increase of satellite peak areas. This implies that the formation of the $\lambda$ phase is taking place in the already precipitated Mo clusters in grain boundary regions. This is further corroborated by carrying out a heat treatment at a high temperature of 1100°C for the $x = 0.015$ alloy (earlier heat treated at 520°C for 24 h in which the satellite intensity decreased due to Mo clustering). The Mössbauer spectra and the hmf distributions for this heat-treated sample are similar to the disordered as-milled alloy showing that the Mo clusters dissolve into the matrix when the grain sizes became microcrystalline which was also confirmed by the line width of the X-ray diffraction pattern recorded for this sample.

### 3.3. $DO_3 \rightarrow L1_2$ structural transformation in $Fe_3Ge$

An interesting structural phase transformation behaviour was observed by Zhou and Bakker [15] during mechanical milling of $L1_2$ ordered $Fe_3Ge$ alloy. The fcc based $L1_2$ structure was first atomically disordered for short periods of milling (about 2 h) as seen by the disappearance of super-lattice reflections, but later transformed to a disordered bcc structure on further milling. Thus there was not only chemical disorder induced as a result of milling as is usually the case with other ordered alloys but also a structural change driven by mechanical milling. We studied the synthesis and phase transformation behavior of $Fe_3Ge$ alloys by direct milling of the constituent elements and found several new and interesting effects. The as-milled material forms in a disordered bcc $\alpha$ phase (A2 structure), orders initially into the $\alpha_1$ phase ($DO_3$ structure) on isothermal heating and later transforms to the equilibrium $\varepsilon'$ phase ($L1_2$ structure).

The X-ray diffraction patterns and HMF distributions from Mössbauer spectra of $Fe_{0.75}Ge_{0.25}$ and $Fe_{0.73}Ge_{0.27}$ alloy synthesized by mechanical alloying of the elemental powders showed the formation of these alloys in disordered bcc $\alpha$ phase (A2). According to the equilibrium phase diagram [16] however the $Fe_{1-x}Ge_x$ alloy system should have a $\alpha_1$-phase region for $0.16 \leq x \leq 0.21$ and a two-phase region ($\alpha_1 + \beta$) for $0.21 \leq x \leq 0.37$.

The phase diagram for Fe-Ge alloy system shows an $\varepsilon'$ phase ($L1_2$ order) around $x = 0.25$ composition at temperatures above 400°C. We heat treated the $x = 0.27$ as milled alloy at a temperature of 520°C to see the evolution of this ordered $L1_2$ phase from the disordered bcc (A2) phase. The evolution of the field

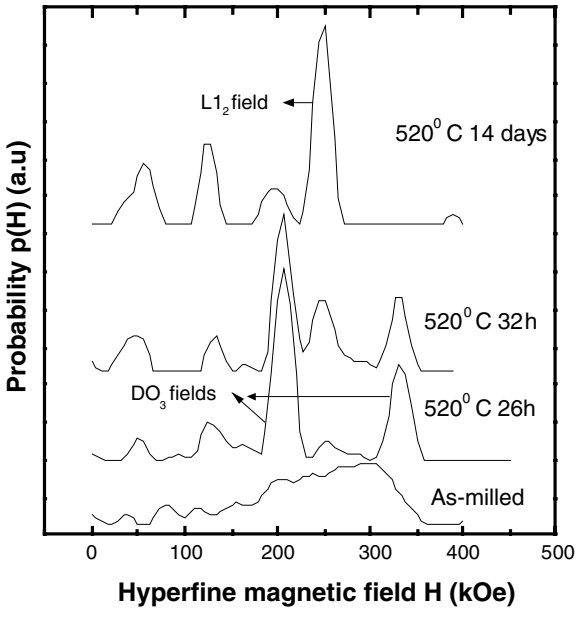


*Figure 3* Hyperfine magnetic field distributions evaluated from the Mössbauer spectra showing the evolution of distinct peaks due to the $\alpha_1$ and $\varepsilon'$ phases at different times.

distributions is shown in Fig. 3. In the initial stages of the transformation there is formation of $\alpha_1$ phase as can be seen unambiguously by the presence of 330 and 205 kOe peaks in the HMF distribution, characteristic of $DO_3$ phase [17]. The $\varepsilon'$ phase is seen to develop rapidly only after a time of 32 h as seen from the presence of peaks in HMF distributions at 245 kOe. Simultaneously there is a decrease in the intensity of the peaks corresponding to the $\alpha_1$ phase. X-ray diffraction studies also confirm the presence of $\varepsilon'$ ($L1_2$) phase by the presence of (111) and (110) reflections from this phase.

We proposed [17] that this phase transformation behavior from the disordered bcc $\alpha$ phase to the equilibrium $\varepsilon'$ ($L1_2$) phase through a metastable ordered $\alpha_1$ ($DO_3$) phase is also a consequence of the Gibbs Thomson effect. The Gibbs free energy of an alloy phase increases by an amount $\Delta G \cong 2\gamma V_m/R$ (Equation 1) for a finite size grain of radius R (assuming spherical grains) relative to a very large size system due to the surface energy $\gamma$ residing in the grain boundary:

$$G(R) \cong G(\infty) + 2\gamma V_m/R \tag{4}$$

For finite size grains the Gibbs free energy for the $DO_3$ grains as well as the $L1_2$ grains will be increased relative to their bulk Gibbs free energy. However due the close packing of the fcc grains the grain boundary energy for the $L1_2$ grains is larger as compared to the $DO_3$ grains and the increase in Gibbs free energy of $L1_2$ grains will be more as compared to the $DO_3$ grains. The lower Gibbs free energy $DO_3$ ordered phase is therefore stabilized for smaller grain size in the initial stages of transformation. However as the grains grow in size the Gibbs free energy of the $L1_2$ ordered phase decreases faster than the Gibbs free energy of the $DO_3$ ordered phase and they both become equal at a certain grain size $R_0$. Beyond $R_0$ Gibbs free energy of the $L1_2$

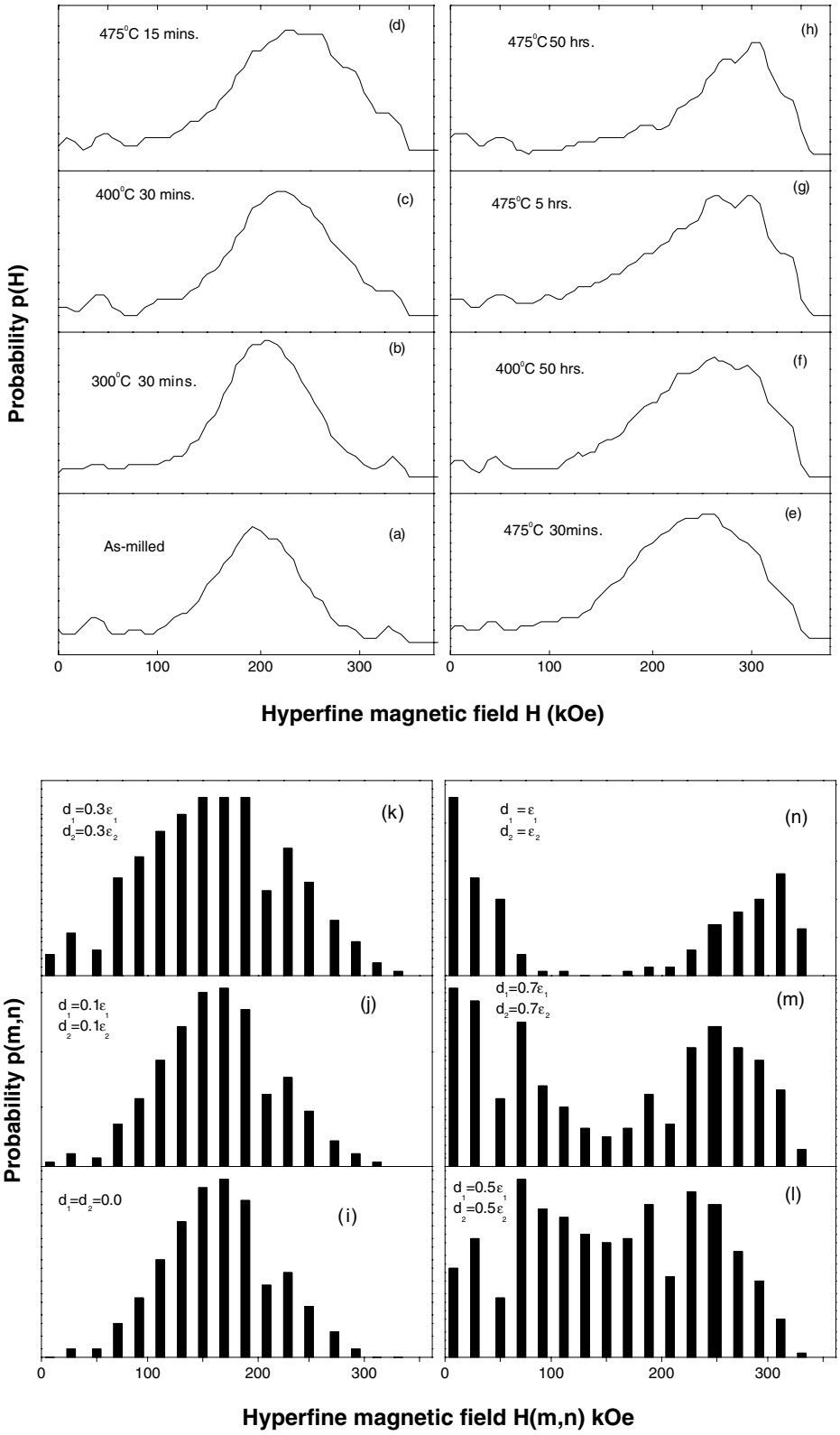


*Figure 4* Insets (a) to (h) show the experimental hyperfine magnetic field distributions for $Fe_{0.55}Cr_{0.45}$ alloy evaluated at different temperatures and times as mentioned against them; '$m$' and '$n$' represent the number of 1st and 2nd Cr nearest neighbours of Fe. Insets (i) to (n) show the simulated probability distributions for various stages of spinodal decomposition represented by the deviations $d_1$ and $d_2$ from the initial composition in terms of $\varepsilon_1$ and $\varepsilon_2$, the distances between the starting composition and the phase boundaries of the Fe-rich and Cr-rich phases respectively.

ordered phase is lower than that of the $DO_3$ ordered phase and there is a rapid phase transformation to the $L1_2$ phase. The value estimated by us [17] for $R_0$ from thermodynamic considerations was found to be ∼12 nm which is of the same order as the experimental value of ∼22 nm.

### 3.4. Spinodal decomposition in Fe-Cr alloys

Nanocrystalline $Fe_{1-x}Cr_x$ ($x = 0.1, 0.2, 0.35, 0.45$) alloys were prepared by mechanical alloying. Single A2 phase (disordered bcc) homogeneous alloys were formed after typical milling times of 24–30 h as confirmed by powder X-ray diffraction and Mössbauer

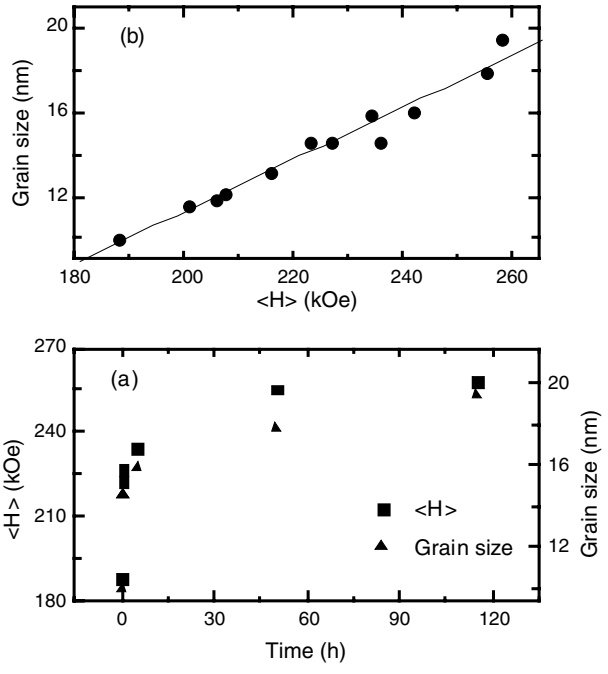


*Figure 5* (a) Temporal evolution of average hyperfine magnetic field ($\langle H \rangle$) and grain size. (b) Parametric plot showing temperature independent linear co-relation between grain size and $\langle H \rangle$.

spectroscopic studies. To study the spinodal phase decomposition behaviour, the as-milled alloys were heat treated at 475, 460, 400 and 300°C for various periods of times ranging from few minutes to hundreds of hours.

The average grain sizes of the as-milled samples were found to be ∼10 nm. Fig. 4a shows the representative hmf distribution of the as-milled alloy with 45 at.% Cr as obtained from the Mössbauer spectrum. This distribution shows a one-to-one correspondence with the binomial distribution (shown in Fig. 4i) expected for a random configuration of atoms in a disordered bcc alloy. This result was corroborated by the X-ray result, in which only bcc lines corresponding to Fe-Cr alloy were present without any signature of Fe-rich ($\alpha$) and Cr-rich ($\alpha'$) phases. Average hmf, $\langle H \rangle$, derived from the Mössbauer spectra was suggested as a very good method of finding whether the phase decomposition reaction proceeds through nucleation and growth (NG) or spinodal decomposition (SD) [18]. Fig. 5a shows the temporal evolution of $\langle H \rangle$ and grain size at 475°C for the 45 at.% Cr alloy. The immediate rise in $\langle H \rangle$ with time is a clear indication that the reaction proceeds through spinodal decomposition [18]. In case of 35 at.% Cr also the result is similar but in case of 10 at.% and 20 at.% Cr samples, the $\langle H \rangle$ at 400 and 460°C is nearly constant with time showing clearly that the NG process is taking place in these alloys as expected from the phase diagram.

We adopted a simple-minded model of composition fluctuation due to spinodal decomposition in the form of Gaussian composition profiles centered at compositions $x_0 \pm \Delta x$ (where $x_0$ is the starting composition) and found out the probability distributions at different stages of the decomposition. Fig. 4a–h and i–n show the experimental and simulated probability distributions respectively, for the 45 at.% Cr alloy. The initial broadening of the distributions is once again a clear indication of the SD process occurring in the system. The final degree of decomposition obtained using the method of Dubiel [18] was 0.54 at 475°C, which was of the same order of magnitude as obtained for the polycrystalline alloy. However, the interesting result that emerges from our study is that the grain growth is linearly co-related to $\langle H \rangle$. Fig. 5b shows a parametric plot between grain size and $\langle H \rangle$, which includes data points for all temperatures. This implies that the phase formation through the SD process is limited to a spatial region of the order of the nanocrystalline grain size. The driving force which controls both the processes could be the decrease in Gibbs' free energy through decrease in the interfacial gradient energy, which is responsible for the spatial extent of the composition fluctuation domains [Ref. [1], p. 312].

## 4. Conclusions

We have shown above how the nanocrystalline nature of alloys significantly influences the behavior of the different metallurgical phase transformations. The large fraction of grain boundary regions provides short-circuited diffusion paths for atom movements and this seems to be the dominant mechanism for chemical order disorder transformation [5, 19]. The substantial surface energy contribution to the Gibbs free energy changes the phase stability of the alloy system in the nanophase state and affects the structural phase transformation [17]. A concept of negative surface energy for binary alloy systems with repulsive A-B interactions was introduced to understand the correlation between grain size and grain boundary segregation in the precipitation phase transformation [20]. Finally, we observed that for the spinodal decomposition process in a nanocrystalline system the growth of composition fluctuation regions was correlated to the growth of grains in the system [21].

## References

1. D. A. PORTER and K. E. EASTERLING, in "Phase Transformations in Metals and Alloys," 2nd ed. (Chapman and Hall, London, 1992).
2. B. FULTZ, *Acta Metall.* **37** (1989) 823.
3. *Idem.*, *Hyperfine Interactions* **41** (1988) 607.
4. B. FULTZ, H. H. HAMDEH and D. H. PEARSON, *Acta Metall.* **37** (1989) 2841.
5. S. SARKAR and C. BANSAL, *Acta Mater.* **49** (2001) 1789.
6. S. SARKAR, N. CHAKROBARTY and C. BANSAL, *Solid State Physics (India)* **41** (1998) 203.
7. M. B. STEARNS, *Phys. Rev.* B **147** (1966) 439.
8. I. VINCZE and A. T. ALDRED, *ibid.* **9** (1974) 3845.
9. BEN DE'MAYO, *ibid.* **24** (1981) 6503.
10. A. R. MIEDEMA, P. F. DE'CHATEL and F. R. DE'BOER, *Physica* B **100** (1980) 1.
11. G. E. MURCH, in "Phase Transformations in Materials," edited by R. W. Cahn, P. Haasen and E. J. Kramer (VCH, Weinheim, 1991) p. 90.
12. H. L. MARCUS, M. E. FINE and L. H. SCHWARZ, *J. Appl. Phys.* **38** (1967) 4750.
13. H. L. MARCUS and L. H. SCHWARZ, *Phys. Rev.* **62** (1967) 259.
14. C. BANSAL, Z. Q. GAO and B. FULTZ, *Nanostruct. Mater.* **5** (1995) 327; S. SARKAR and C. BANSAL, *J. Alloys Compd.* **366** (2004) 107.
15. G. F. ZHOU and H. BAKKER, *Europhys. Lett.* **30** (1995) 433.

16. T. B. MASSALSKI (ed.), "Binary Alloy Phase Diagrams" (ASM International, Metals Park, OH, 1990).
17. S. SARKAR, C. BANSAL and ASHOK CHATTERJEE, *Phys. Rev.* B **62** (2000) 3218.
18. J. CIEŚLAK, S. M. DUBIEL and B. SEPIOL, *J. Phys.: Condens. Matter* **12** (2000) 6709.
19. S. SARKAR and C. BANSAL, *J. Alloys Compd.* **334** (2002) 135.
20. *Idem.*, *J. Nanosci. Nanotech.* **4** (2004) 203.
21. *Idem.*, Presented at the Conference on "Recent Developments and Challenges in Physics" (Hyderabad, December 19–22, 2002).

*Received 11 September 2003*
*and accepted 27 February 2004*